

# Electromagnetic ITG Modes in Helical Systems

KURODA Tohru<sup>1</sup> and SUGAMA Hideo<sup>1,2</sup>

<sup>1</sup>National Institute for Fusion Science, Toki 509-5292, Japan

<sup>2</sup>Graduate University for Advanced Studies, Toki 509-5292, Japan

(Received: 14 December 2001 / Accepted: 3 June 2002)

## Abstract

Linear properties of electromagnetic ion temperature gradient (ITG) modes in toroidal helical systems are studied. The collisionless ion gyrokinetic equation and the massless-electron assumption are used to derive two coupled integral eigenmode equations for the electrostatic potential and the parallel component of the vector potential from the quasineutrality condition and the Amère's law. Based on a model magnetic configuration for the Large Helical Device (LHD), the real frequencies, growth rates, and eigenfunctions of the ITG mode are obtained by numerically solving the integral eigenmode equations. Effects of  $\beta$  = (plasma pressure/magnetic pressure) on the ITG mode are investigated and compared with those in the tokamak case.

## Keywords:

ITG mode, helical system, high  $\beta$  plasma, gyrokinetic equation

## 1. Introduction

The ion temperature gradient (ITG) mode is considered to cause the anomalous ion thermal transport in high temperature core regions of tokamak plasmas [1]. Recently, helical systems such as the Large Helical Device (LHD) [2] have succeeded in producing high ion temperature plasmas, and there have been several theoretical studies on the electrostatic ITG mode in helical systems [3-6]. In addition, experiments to produce higher  $\beta$  plasmas in helical systems are in progress, and therefore it is important to clarify electromagnetic effects on the ITG mode. The finite- $\beta$  effects on the ITG mode in tokamak plasmas has been investigated by Dong *et al.* [7]. In this work, linear properties of the electromagnetic ITG mode in finite- $\beta$  helical systems are studied and compared with those in the electrostatic case and in the tokamak case.

The spatial distribution of the magnetic field strength in a large-aspect-ratio toroidal helical system is written as

$$B/B_0 = 1 - \varepsilon_t \cos \theta - \varepsilon_h \cos (L\theta - M\zeta), \quad (1)$$

where  $B_0$  is the magnetic field strength on the magnetic axis,  $\theta$  and  $\zeta$  represent the poloidal and the toroidal angles, respectively, and  $L$  and  $M$  are the poloidal and toroidal period numbers of the helical fields, respectively. For example,  $L = 2$  and  $M = 10$  for the LHD.  $\varepsilon_t \propto r$  and  $\varepsilon_h \propto r^L$  with the minor radius  $r$  represent the parameters associated with the toroidicity and helicity, respectively. In helical systems, characteristics of the ITG mode are influenced by the existence of the helical magnetic component and the negative magnetic shear in contrast to the toroidal symmetry and the positive magnetic shear in conventional tokamaks.

## 2. Eigenmode Equations

In this section, two coupled integral eigenmode equations for the linear electromagnetic ITG mode in helical systems, which are similar to those of Dong *et al.*, are presented. The temporal dependence of the perturbation terms  $\tilde{\phi}$  (the electrostatic potential)  $\tilde{A}_{\parallel}$  (the parallel component of the vector potential) is assumed to

Corresponding author's e-mail: tkuroda@nifs.ac.jp, sugama@nifs.ac.jp

be given by  $\tilde{\phi}, \tilde{A}_{\parallel} \propto \exp(-i\omega t)$  with a complex frequency  $\omega = \omega_r + i\gamma$  and time  $t$ . The distribution functions for species  $a = i(\text{ion}), e(\text{electron})$  are written as  $f_a = nF_{Ma} + \delta f_a$  (hereafter, the subscript  $a$  is omitted for simplicity except where it is necessary). Here, the equilibrium part is assumed to be the Maxwellian distribution function  $F_M = \pi^{-3/2} v_T^{-3} \exp(-v^2/v_T^2)$ , where the thermal velocity is given by  $v_T = (2T/m)^{1/2}$  with the equilibrium temperature  $T$  and the mass  $m$  for each species. The perturbation part is given by  $\delta f = -(q_c \phi / T) n F_M + \tilde{h} \exp(-ik_{\perp} \cdot \rho)$ , where  $\rho \equiv (\mathbf{B}/B \times (\mathbf{v}/\Omega_B))$  is the gyroradius vector,  $\Omega_B = q_c B/(mc)$  is the gyrofrequency,  $\mathbf{k}$  is the wavenumber vector,  $q_c$  is the charge ( $q_c = e$  for ions,  $-e$  for electrons),  $n$  is the equilibrium density, and  $c$  is the light speed. The nonadiabatic part of the distribution function  $\tilde{h}$ , is determined by the collisionless linear electromagnetic gyrokinetic equation,

$$\left[ i \frac{v_{\parallel}}{Rq} \frac{\partial}{\partial \theta} + (\omega - \omega_D) \right] \tilde{h} = (\omega - \omega_{*T}) J_0 \left( \frac{k_{\perp} v_{\perp}}{\Omega_B} \right) F_M \frac{q_c n}{T} \left( \tilde{\phi} - \frac{v_{\parallel}}{c} \tilde{A}_{\parallel} \right), \quad (2)$$

where  $\omega_D = \mathbf{k}_{\perp} \cdot \mathbf{v}_D$ ,  $\mathbf{v}_D = \Omega_B^{-1} (v_{\parallel}^2 + v_{\perp}^2/2) \mathbf{B}^{-2} \mathbf{B} \times \nabla B$ ,  $\omega_{*T} = \omega_* [1 + \eta(v/v_T) - 3/2]$ ,  $\omega_* = ck_{\theta} T / q_c B L_n$ ,  $\eta \equiv L_n / L_T$ ,  $L_n = -(d/dr) \ln n$ , and  $L_T = -(d/dr) \ln T$ . In the case of the toroidal helical configuration given by eq. (1), the magnetic drift frequency is given by

$$\omega_D = 2(L_n / r) \omega_{*i} (v_{\parallel}^2 + v_{\perp}^2/2) / v_{Ti}^2 \times \left[ \varepsilon_i \{ \cos \theta + [\hat{s}(\theta - \theta_k) - \alpha_p \sin \theta] \sin \theta \} + L \varepsilon_n \{ \cos(L\theta - M\zeta) + [\hat{s}(\theta - \theta_k) - \alpha_p \sin \theta] \sin(L\theta - M\zeta) \} \right], \quad (3)$$

where  $\hat{s} = (r/q) dq/dr$  is the magnetic shear parameter. Here,  $\mathbf{k}_{\perp} = k_{\alpha} (\nabla_{\alpha} + \theta_k \nabla q)$  is the perpendicular wavenumber vector given by the ballooning representation [8], where  $q(r)$  is the safety factor,  $\alpha = \zeta - q\theta$  is the label of the magnetic field line, and  $k_{\alpha} = -n_i$  represents the toroidal mode number, which is related to the poloidal wavenumber as  $k_{\theta} = n_i q/r$ .

In order to derive the eigenmode equations, the quasineutrality condition

$$\tilde{n}_i = \tilde{n}_e, \quad (4)$$

and the Ampère's law

$$\nabla_{\perp}^2 \tilde{A}_{\parallel} = -\frac{4\pi}{c} (\tilde{j}_{i\parallel} + \tilde{j}_{e\parallel}), \quad (5)$$

are used. The number density perturbation  $\tilde{n} = \int d^3v \delta f$  and the current density perturbation  $\tilde{j}_{\parallel} = q_c \int d^3v v_{\parallel} \delta f$  are rewritten in terms of  $\tilde{\phi}$  and  $\tilde{A}_{\parallel}$  by integrating eq. (2). Here, we neglect effects of trapped particles and take the lowest-order solution of eq. (2) in the massless-electron approximation. The resultant integral equations for the electromagnetic ITG mode are given by

$$(1 + \tau_e) \tilde{\phi}(k) = \int_{-\infty}^{\infty} \frac{dk'}{\sqrt{2\pi}} \left[ K_{11}^i(k, k') \tilde{\phi}(k') + \{K_{12}^i(k, k') + K_{12}^e(k, k')\} \tilde{A}_{\parallel}(k') \right], \quad (6)$$

and

$$\frac{1}{2\tau_e} \tilde{A}_{\parallel}(k) = \int_{-\infty}^{\infty} \frac{dk'}{\sqrt{2\pi}} \left[ \{K_{21}^i(k, k') K_{21}^e(k, k')\} \tilde{\phi}(k') + \{K_{22}^i(k, k') + K_{22}^e(k, k')\} \tilde{A}_{\parallel}(k') \right], \quad (7)$$

where

$$K_{11}^i(k, k') = -i \int_{-\infty}^0 \omega_{*e} d\tau \bar{K}(k, k', \tau), \quad (8)$$

and

$$K_{12}^i(k, k') = -i \int_{-\infty}^0 \omega_{*e} d\tau \frac{-1}{2\sqrt{a}\lambda} (k - k') \bar{K}(k, k', \tau), \quad (9)$$

$$K_{21}^i(k, k') = -i \int_{-\infty}^0 \omega_{*e} d\tau \frac{\beta_i}{2\tau_e \sqrt{a}\lambda} (k - k') \bar{K}(k, k', \tau), \quad (10)$$

$$K_{22}^i(k, k') = -i \int_{-\infty}^0 \omega_{*e} d\tau \frac{-\beta_i}{4\tau_e \sqrt{a}\lambda} (k - k')^2 \bar{K}(k, k', \tau), \quad (11)$$

$$K_{12}^e(k, k') = i \frac{q\sqrt{\pi}\tau_e}{2\sqrt{2}\varepsilon_n \hat{s}} \left( \frac{\omega}{\omega_{*e}} - 1 \right) \text{sgn}(k - k'), \quad (12)$$

$$K_{21}^e(k, k') = -\frac{\beta_i}{\tau_e} K_{12}^e(k, k'), \quad (13)$$

$$K_{22}^e(k, k') =$$

$$\beta_i \left[ -\frac{\sqrt{\pi}}{4\sqrt{2}} \left( \frac{q}{\varepsilon_n \hat{s}} \right)^2 \frac{\omega}{\omega_{*e}} \left( \frac{\omega}{\omega_{*e}} - 1 \right) |k - k'| + \frac{\sqrt{\pi} q^2 k_{\theta}}{2\sqrt{2} \hat{s} \varepsilon_n} \left\{ \frac{\omega}{\omega_{*e}} - (1 + \eta_e) \right\} \text{sgn}(k - k') g(\theta, \theta') \right], \quad (14)$$

and

$$\bar{K}(k, k', \tau) = \frac{\sqrt{2}e^{-i\omega\tau}}{\sqrt{a}(1+a)\sqrt{\lambda}} e^{-(k-k')^2/4\lambda} \times \left[ \frac{\omega}{\omega_{*e}} \tau_e + 1 - \frac{3}{2} \eta_i + \frac{\eta_i(k-k')^2}{4a\lambda} + \frac{2\eta_i}{(1+a)} \right] \left[ 1 - \frac{k_{\perp}^2 - k'_{\perp}{}^2}{2(1+a)\tau_e} + \frac{k_{\perp}k'_{\perp}}{(1+a)\tau_e} \frac{I_1}{I_0} \right] \Gamma_0(k_{\perp}, k'_{\perp}). \quad (15)$$

Here,  $g(\theta, \theta') = \int_{\theta'}^{\theta} d\theta'' G_c(\theta'')$  with  $G_c = \omega_{Ti}/[2(L_n/r) \varepsilon_i \omega_{*i} (v_{\parallel}^2 + v_{\perp}^2/2)/v_{Ti}^2]$  using eq. (3),  $\lambda = (\tau^2 \omega_{*e}^2 / \tau_e a) (\hat{s} \varepsilon_n / q)^2$ ,  $a = 1 + i(2\varepsilon_n / \tau_e) \omega_{*e} \tau g(\theta, \theta') / (\theta - \theta')$ ,  $\beta_i = 8\pi n T_i / B^2$ ,  $\beta = \beta_i (1 + \tau_e)$ ,  $k = k_{\theta} \hat{s}(\theta - \theta_k)$ ,  $k' = k_{\theta} \hat{s}(\theta' - \theta_k)$ ,  $k_{\perp}^2 = k_{\theta}^2 [1 + (\hat{s}(\theta - \theta_k) - \alpha_p \sin \theta)^2]$ ,  $k'_{\perp}{}^2 = k_{\theta}^2 [1 + (\hat{s}(\theta' - \theta_k) - \alpha_p \sin \theta')^2]$ ,  $\alpha_p = -R_0 q^2 (d\beta/dr) = (q^2 \beta_i / \varepsilon_n) (1 + \tau_e) (1 + \eta_i)$ , and  $\varepsilon_n = L_n / R_0$  ( $R_0$ : the major radius). In eqs. (6) and (7),  $\tilde{\phi}$ ,  $\tilde{A}_{\parallel}$ , and  $k$  are normalized by  $T_e/e$ ,  $(T_e/e)(c/v_{Ti})$ , and  $\rho_s^{-1} = eB/(c\sqrt{m_i T_e})$ , respectively. For evaluating  $k_{\perp}$ , we have used the  $s$ - $\alpha$  equilibrium model [9]. An explicit form of  $a$  is given by

$$a = 1 - i2(L_n/r)\tau_e^{-1}\omega_{*e}\tau/(\theta - \theta') \times \left( \varepsilon_i \left[ (\hat{s} + 1)(\sin \theta - \sin \theta') - \hat{s} \left\{ (\theta - \theta_k) \cos \theta - (\theta' - \theta_k) \cos \theta' \right\} - \frac{\alpha_p}{2} \left\{ (\theta - \theta') - (\sin \theta \cos \theta - \sin \theta' \cos \theta') \right\} \right] + (L \varepsilon_n) \left[ \frac{\hat{s}(L - Mq)^{-1} + 1}{L - Mq} \times \left\{ \sin((L - Mq)\theta - M\alpha) - \sin((L - Mq)\theta' - M\alpha) \right\} - \frac{\hat{s}}{L - Mq} \left\{ (\theta - \theta_k) \cos((L - Mq)\theta - M\alpha) - (\theta' - \theta_k) \cos((L - Mq)\theta' - M\alpha) \right\} + \frac{\alpha_p}{2} \left( \frac{1}{L - Mq + 1} \left\{ \sin([L - Mq + 1]\theta - M\alpha) - \sin([L - Mq + 1]\theta' - M\alpha) \right\} - \frac{1}{L - Mq - 1} \left\{ \sin([L - Mq - 1]\theta - M\alpha) - \sin([L - Mq - 1]\theta' - M\alpha) \right\} \right) \right] \right). \quad (16)$$

It should be noted that  $K_{21}$  and  $K_{22}$  are proportional to  $\beta_i$ , which represents that the electromagnetic component given by  $\tilde{A}_{\parallel}$  appears only for finite  $\beta_i$ . Our previous work on the electrostatic ITG mode [3] is reproduced in the limit  $\beta_i \rightarrow 0$ . By solving the integral eigenmode eqs. (6) and (7), the parameter dependence of the dispersion relation is obtained as

$$\frac{\omega}{\omega_{*e}} = F(q, \hat{s}, \theta_k, \alpha, k_{\theta}, \eta_i, \eta_e, \varepsilon_n, \alpha_p, \tau_e, \varepsilon_n/\varepsilon_i, L, M), \quad (17)$$

where  $F$  is a dimensionless function.

### 3. Numerical Results

Here, we use the standard parameters of our previous work [3], which are given by  $q = 2$ ,  $\hat{s} = -1$  (negative shear),  $\theta_k = 0$ ,  $\alpha = 0$ ,  $k_{\theta p T_i} = 0.65$ ,  $\eta_i = \eta_e = 3$ ,  $\varepsilon_n = 0.3$ ,  $\tau_e = 1$ ,  $\varepsilon_n/\varepsilon_i = 1$ ,  $L = 2$ ,  $M = 10$ . For the tokamak case,  $\varepsilon_n/\varepsilon_i = 0$ .

Figure 1 shows the  $\beta_i$  dependence of the real frequency and the growth rate of the ITG mode. For  $\beta_i = 0.001\%$  and  $0.5\%$ , the real and imaginary parts of the eigenfunctions  $\tilde{\phi}$  and  $\tilde{A}_{\parallel}$  are plotted in Fig. 2 for the negative shear tokamak case and in Fig. 3 for the helical system. For both tokamak and helical cases, the low  $\beta_i$  case ( $\beta_i = 0.001\%$ ), the real frequency, the growth rate, and the potential eigenfunction are in good agreement with those in the electrostatic case [3], and the amplitude of  $\tilde{A}_{\parallel}$  is negligibly small. As shown in Figs. 2(c),(d) and 3(c),(d), the magnetic fluctuation  $\tilde{A}_{\parallel}$  grows due to finite  $\beta_i$ , which also adds some deformations to the electrostatic potential. This represents the coupling to electromagnetic shear Alfvén waves [7], and gives stabilization effects to the ITG mode for both tokamak and helical cases with  $\beta_i$  increased as seen in Fig. 1(a).

Comparing the profiles of the eigenfunctions in Figs. 2 and 3, the eigenfunctions for the helical case are

more oscillatory due to the helical magnetic ripples than those for the tokamak case. In the helical system, these oscillations in the eigenfunctions, which are more enhanced for higher  $\beta_i$ , increase the effective parallel wavenumber, decrease the parallel phase velocity, and

accordingly strengthen the ion Landau damping. Also, the helical magnetic ripples reduce the bad curvature region in the outside of the torus [3]. Thus, the growth rates of the ITG mode are smaller for the helical system as shown in Fig. 1(a), where the complete stabilization occurs at  $\beta_i \approx 0.8\%$ .

#### 4. Summary

In this work, we have investigated electromagnetic effects on the linear ITG mode in helical systems with finite  $\beta$ . Higher  $\beta$  increases magnetic fluctuations and gives more oscillatory profiles of eigenfunctions, which results from the multiplier effect of the helical magnetic ripples and the coupling to electromagnetic shear Alfvén waves. Thus, the growth rate of the ITG mode for the helical system decreases with increasing  $\beta_i$  and keeps smaller values than for the tokamak case.

Here, effects of collisions, trapped particles, impurities, and sheared electric fields are not taken into account. Also, another branch of unstable modes, which is associated with the kinetic Alfvén mode, was discovered by Dong *et al.* [7] although it is not found here yet. These subjects remain as future tasks.

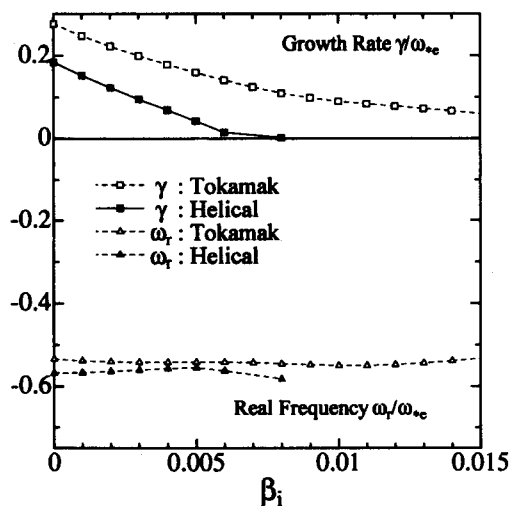


Fig. 1 Normalized real frequency  $\omega_r/\omega_{*e}$  and growth rate  $\gamma/\omega_{*e}$  as a function of  $\beta_i$  for  $q = 2$ ,  $\hat{s} = -1$ ,  $\theta_k = 0$ ,  $\alpha = 0$ ,  $k_{\theta\pi} = 0.65$ ,  $\eta_i = \eta_e = 3$ ,  $\varepsilon_n = 0.3$ , and  $\tau_e = 1$ . Here  $\varepsilon_n/\varepsilon_t = 0$  for the tokamak case, and  $\varepsilon_n/\varepsilon_t = 1$ ,  $L = 2$ ,  $M = 10$  for the helical system.

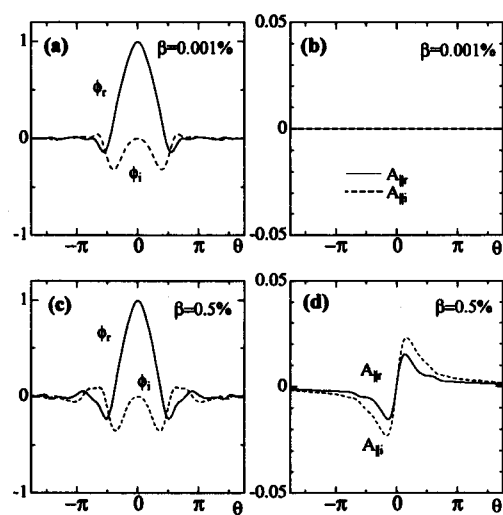


Fig. 2 Normalized eigenfunctions  $e\tilde{\phi}/T_e$  and  $ev_{Ti}\tilde{A}_i/cT_e$  in the tokamak case with  $\varepsilon_n/\varepsilon_t = 0$ , for  $q = 2$ ,  $\hat{s} = -1$ ,  $\theta_k = 0$ ,  $\alpha = 0$ ,  $k_{\theta\pi} = 0.65$ ,  $\eta_i = \eta_e = 3$ ,  $\varepsilon_n = 0.3$  and  $\tau_e = 1$  for two cases of  $\beta_i = 0.001\%$  [(a),(b)] and  $\beta_i = 0.5\%$  [(c),(d)]. The horizontal axis represents the covering space of the ballooning angle  $\theta$ .

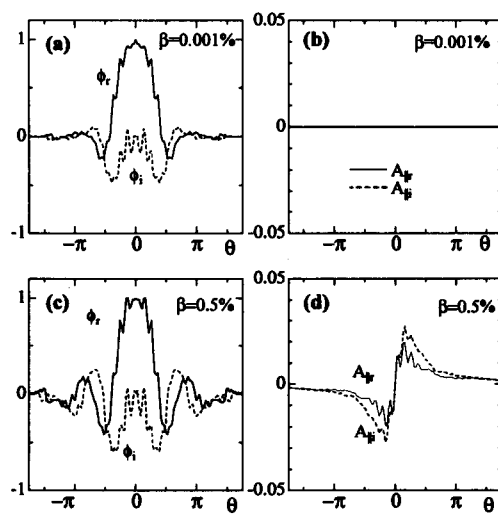


Fig. 3 Normalized eigenfunctions  $e\tilde{\phi}/T_e$  and  $ev_{Ti}\tilde{A}_i/cT_e$  in the helical system with  $\varepsilon_n/\varepsilon_t = 1$ ,  $L = 2$ ,  $M = 10$  for  $q = 2$ ,  $\hat{s} = -1$ ,  $\theta_k = 0$ ,  $\alpha = 0$ ,  $k_{\theta\pi} = 0.65$ ,  $\eta_i = \eta_e = 3$ ,  $\varepsilon_n = 0.3$ , and  $\tau_e = 1$  for two cases of  $\beta_i = 0.001\%$  [(a),(b)] and  $\beta_i = 0.5\%$  [(c),(d)]. The horizontal axis represents the covering space of the ballooning angle  $\theta$ .

### Acknowledgement

The authors thank Prof. J.Q. Dong and Dr. G. Rewoldt for useful discussion during their visit to NIFS. They also appreciate useful comments of Prof. K. Itoh on this work.

### References

- [1] W. Horton, *Rev. Mod. Phys.* **71**, 735 (1999).
- [2] H. Yamada *et al.*, *Nucl. Fusion* **41**, 901 (2001).
- [3] T. Kuroda *et al.*, *J. Phys. Soc. Jpn.* **69**, 2485 (2000).
- [4] G. Rewoldt *et al.*, *Phys. Plasmas* **7**, 4942 (2000).
- [5] J.L.V. Lewandowski, *Plasma Phys. Control. Fusion* **40**, 283 (1998).
- [6] T. Kuroda and H. Sugama, *J. Phys. Soc. Jpn.* **70**, 2235 (2001).
- [7] J.Q. Dong *et al.*, *Nucl. Fusion* **39**, 1041 (1999).
- [8] R.L. Dewar and A.H. Glasser, *Phys. Fluids* **26**, 3038 (1983).
- [9] J.W. Connor *et al.*, *Phys. Rev. Lett.* **40**, 396 (1978).